14th International Symposium on Turbulence and Shear Flow Phenomena (TSFP14)
Heidelberg, Germany, July 28–31, 2026

EFFECT OF WALL HEATING AND HIGH ENTHALPY ON SEPARATION IN HYPERSONIC SHOCK BOUNDARY LAYER INTERACTION

Vijaya Lahari, Soorya Sridhar, Harsha Rathi and Krishnendu Sinha*
Department of Aerospace Engineering
Indian Institute of Technology Bombay, India

ABSTRACT

Hypersonic flows are characterized by strong shock waves, high temperatures, and complex interactions between turbulence and thermo-chemical non-equilibrium effects, with shock–boundary layer interaction (SBLI) often leading to flow separation and the formation of a recirculation bubble. This study systematically investigates the effects of freestream total enthalpy and wall temperature ratio on SBLI, with these parameters varied independently to decouple their individual effects on separation bubble. RANS simulations over a cone–flare geometry are performed for conditions representative of realistic hypersonic flight regimes, extending the parameter space to higher wall temperatures and enthalpy levels. The results show that increasing enthalpy reduces separation bubble size due to higher boundary layer momentum, while increasing wall temperature significantly enlarges the separation region. Interaction length scaling is assessed under these conditions, showing good agreement overall but deviations at higher thermal loads. To examine this, a simplified analytical model is developed to estimate the maximum temperature within the interaction region, enabling identification of regimes where existing scaling remains valid. This work improves understanding of high-enthalpy SBLI and provides a pathway to extend scaling relations to realistic hypersonic flow conditions.

1 INTRODUCTION

Hypersonic flows are characterized by extreme velocities, high temperatures, and complex turbulence–shear interactions, strongly influenced by thermo-chemical non-equilibrium (TCNEQ) effects. In turbulent boundary layers, elevated temperatures intensify processes such as vibrational excitation, species dissociation, and chemical reactions, leading to highly non-linear variations in gas properties and flow dynamics. These processes lag behind the flow as they are not instantaneous and are in non-equilibrium. A key feature of hypersonic viscous flows is shock–boundary layer interaction (SBLI), where adverse pressure gradients can cause boundary layer separation and the formation of a recirculation bubble that governs the strength of the shock system. These phenomena directly impact engine performance, thermal loads, and structural integrity of the aircraft.

Although several studies have examined the effects of Reynolds number, Mach number, wall temperature, and geometry on separation behavior, most focus on low-enthalpy flows where real gas effects are not triggered. At hypersonic speeds, these effects become significant, altering viscosity, thermal conductivity, and the speed of sound, ultimately influencing the flow separation. A detailed understanding of these coupled thermo-chemical and fluid dynamic processes is therefore essential for accurate prediction and control of separation, which is critical for design and performance of hypersonic vehicles.

Recent DNS studies by Duan & Martin (2011) and Volpiani (2021) have provided important insights into hypersonic turbulent boundary layers under TCNEQ conditions, showing increased species dissociation and wall heat flux with rising temperature. Additional work by Passiatore *et al.* (2022) highlights the role of vibrational excitation in amplifying non-equilibrium effects. However, DNS studies remain limited in parameter range due to high computational cost. In contrast, a limited number of RANS-based studies by Jiang *et al.* (2022) and Rathi & Sinha (2024) show that increasing freestream enthalpy reduces separation bubble size, while neglecting real gas effects leads to overprediction. Given the high Reynolds numbers and complex high temperature physics inherent to hypersonic flows, DNS is impractical for engineering applications, and LES remains computationally restricted for parametric studies. RANS approach with a well validated turbulence modeling thus provides a computationally efficient framework for capturing mean flow behavior while incorporating TCNEQ effects, highlighting the need for systematic investigation of SBLI under high-enthalpy conditions.

A number of turbulence models of varying complexity are available in the RANS framework. A judicious choice of the model and a careful validation are essential to get reliable results. Several efforts have been made for validating RANS turbulence models in SBLI flows. Among these, the work of Rathi & Sinha (2024)is particularly relevant for high enthalpy SBLI flows. Their study demonstrates that the shock-unsteadines (SU) modified $k-\omega$ model is capable of accurately predicting separation size over a range of Mach numbers, total enthalpy and wall temperature ratios.

Interaction length scaling is often used to correlate extent of the separation region with flow and thermodynamic parameters through non-dimensional formulations. Rathi & Sinha (2024) proposed a scaling relation that encompasses both low enthalpy and high enthalpy SBLI flows. However, in that study, freestream enthalpy variation was inherently coupled with changes in wall temperature ratio (T_w/T_r), as the dataset was primarily based on experimental test cases, where operating conditions impose such dependencies. As a result, parameters such as Mach number, recovery temperature, and wall thermal state were not independently varied, limiting the ability to isolate their individual effects.

The present study extends the scope of the previous work

*Professor, Department of Aerospace Engineering, IIT Bombay. E-mail: krish@aero.iitb.ac.in

by increasing the enthalpy range to higher values, while independently varying freestream enthalpy and wall temperature ratio by fixing the freestream conditions. This enables clear decoupling of their influences on SBLI.

In this context, the present study performs a systematic RANS-based investigation of hypersonic turbulent SBLI under varying freestream enthalpy and wall temperature conditions, chosen to represent realistic flight regimes. The analysis focuses on characterizing separation behavior through wall pressure and skin friction distributions, followed by an assessment of interaction length scaling in high-enthalpy flows.

A secondary objective is to establish the limits of validity of interaction length scaling in the hypersonic TCNEQ regime. To address this, an extension to the scaling framework is proposed based on estimating the maximum temperature within the interaction region. A simplified analytical approach, combining boundary layer profiles with shock relations, is used to predict peak temperatures and identify conditions where classical scaling remains valid. This enables identification of operating regimes in terms of freestream enthalpy, wall temperature ratio, and flow deflection where the scaling can be reliably applied.

The remainder of the paper is organized as follows. Section-2 describes the test cases considered in the present study. Section-3 outlines the computational domain and grid selection. The numerical methodology, governing approach and the turbulence model chosen for the simulations are presented in Section-4. Section-5 discusses the results and their interpretation. Finally, the key findings and conclusions of the study are summarized in the last section.

2 TEST CASES

The selection of test cases is guided by three complementary considerations: (i) the high-enthalpy cone-flare SBLI configuration studied by Rathi & Sinha (2024), (ii) the gaps identified in prior numerical and theoretical studies on TC-NEQ effects in the SBLI region, and (iii) representative hypersonic flight conditions corresponding to high-speed atmospheric cruise in the mid-stratospheric region (Boyce *et al.* (2003), Kimmel *et al.* (2010)).

The freestream conditions are selected with primary emphasis on total enthalpy, which governs the thermal state of the flow and the onset of thermo-chemical non-equilibrium effects. Most previous studies considered cover enthalpy ranges from 5–25 MJ/kg driven by high Mach numbers and the need to achieve extreme nonequilibrium conditions. In contrast, the present study focuses on the enthalpy range between 0–5 MJ/kg, which is more representative of airbreathing cruise conditions. The chosen conditions are taken from vehicles which typically operate in the Mach 5–8 range at altitudes of approximately 27–50 km. To carry out independent assessment of key parameters, the freestream temperature is anchored at 220 K, corresponding to mid-stratospheric conditions. Within this envelope, the present study considers Mach numbers of $6-8$ which translate to h_0 of $1.81-3.05$ MJ/kg as shown in Table-1.

The selection of wall temperature (T_w) is governed by the wall temperature ratio (T_w/T_r), where T_r is the recovery temperature. Most studies on hypersonic turbulent boundary layers have considered wall temperature ratios of $0.1-0.2$ (Duan & Martin (2011), Volpiani (2021)Passiatore *et al.* (2022), Jiang *et al.* (2022)). While the the absolute wall temperatures in those studies have increased, the wall temperature ratios mostly represent wall cooling conditions rather than heating. Rathi & Sinha (2024) extended these values to a range of $0.15-0.27$. Building on this, the current study parametrically expands T_w/T_r into comparatively hotter regimes. The choice of T_w/T_r is motivated by the fact that hypersonic cruise vehicles are subjected to significant heating, resulting in elevated wall temperatures. Hence wall temperature ratios between 0.15 and 0.6 are considered for this study.

Two primary aspects are investigated: (i) the variation of separation characteristics with changing enthalpy at constant wall temperature ratio, and (ii) the effect of varying wall temperature ratio at constant enthalpy. The cases in the simulation matrix mentioned in Table-1 are named based on the enthalpy (multiplied by 10) followed by the wall temperature ratio (multiplied by 100). Thus, the effect of wall temperature is examined using the cases H24T15, H24T30, and H24T60 at fixed enthalpy of 2.39 MJ/kg, while the effect of enthalpy is isolated by comparing H18T30, H24T30, and H30T30 at a constant wall temperature ratio of 0.3.

We use the cone-flare geometry of Rathi & Sinha (2024) that was well validated against the experimental data. The schematic of the canonical cone flare SBLI geometry is shown in Fig.1. The cone section has a length of 2.37m and a half angle of 7^0, followed by a flare of 0.2m inclined at 33^0 relative to the cone surface. The total axial length of the geometry is 2.5m, with the origin located at an axial distance of 2.353m from the tip of the cone. The test cases considered in Rathi & Sinha (2024) are also listed in Table-1 for comparison.

Table 1. Comparison of hypersonic turbulent SBLI cases (RANS over Cone-flare geometry)

Case Group	**Case**	M_∞	M_e	Re_∞ ($\times 10^6$)	T_w/T_r	T_w **(K)**	h_0 **(MJ/kg)**
	M5H13	4.96	4.52	34.9	0.27	312.6	1.31
	M6H14	6.03	5.37	23.5	0.25	309.1	1.41
Rathi & Sinha (2024)	M8H16	8.03	6.85	12.5	0.23	327.3	1.64
	M6H20	5.90	5.27	36.8	0.19	330.9	1.96
	M8H24	8.10	6.90	10.5	0.16	330.6	2.37
	M7H27	6.92	6.05	12.2	0.15	343.8	2.66
	H18T30	6	5.34	9.62	0.3	493.7	1.81
Present Study	H24T15	7	6.11	11.23	0.15	324	2.39
$T_\infty = 220K$	H24T30	7	6.11	11.23	0.3	648	2.39
$\rho_\infty = 0.0332 kg/m^3$	H24T60	7	6.11	11.23	0.6	1296	2.39
	H30T30	8	6.83	12.83	0.3	826.3	3.05

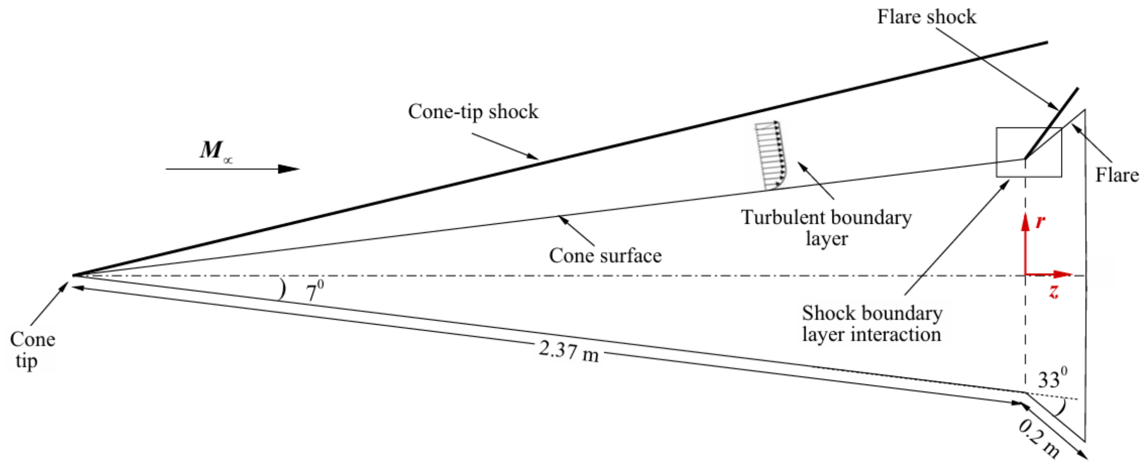

Figure 1. Schematic of cone-flare geometry (Rathi & Sinha (2024))

3 COMPUTATIONAL DOMAIN AND GRID

The computational domain and grid used in the present study are adopted from the reference study. The domain extends from the apex of the cone to the end of the flare in the axial direction, and from the wall of the cone-flare to the outer boundary in the radial direction. The outer boundary is positioned sufficiently far into the freestream to remain outside the influence of shock waves. The boundary conditions for the simulations are taken as isothermal wall at the cone-flare surface, freestream conditions at the inlet and symmetry at the apex of the cone. An extrapolation boundary condition is applied at the outlet.

A grid size of 250 × 150 is used for the the present study, with 250 divisions in the streamwise direction and 150 divisions in the wall-normal direction. The first cell center near the wall is placed at a spacing of 10^{-6} m to adequately resolve near-wall gradients. The mesh, shown in Fig.2, is exponentially stretched, with finer resolution near the apex, the flare corner, and the wall region.

3.1 Validation of Computational Setup

To validate the present work against Rathi & Sinha (2024), a case closely matching the M7H27 condition, corresponding to a wall temperature ratio of 0.15 is selected. The corresponding case in the present study is denoted as H24T15. The variations in density, freestream temperature and wall temperature between the two cases are 15.7%, 12% and 5.6%, respectively.

Fig.3 shows a good agreement in key flow features, including the onset of separation, the minimum C_f and reattachment. Minor deviations in the peak and recovery regions, with a maximum variation of less than 5%, are attributed to slight differences in inlet and wall conditions and the grid. Overall, the agreement confirms the adequacy of the numerical setup and grid resolution. Therefore, the 250 × 150 grid is adopted for the present study, offering a significant reduction in computational time while maintaining accuracy.

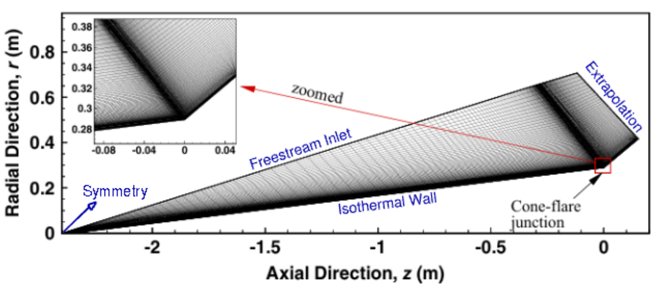

Figure 2. Computational mesh with a zoomed view of the flare corner and boundary conditions

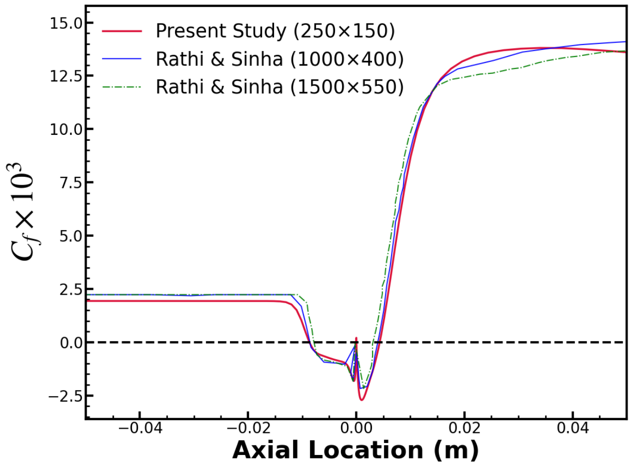

Figure 3. Comparison of C_f across different grid resolutions for case H24T15 with M7H27 of Rathi & Sinha (2024)

4 METHODOLOGY

A well validated in-house code is employed to solve the Reynolds-Averaged Navier–Stokes (RANS) equations coupled with an SU-modified k–ω turbulence model. The shock-unsteadiness (SU) model is specifically tailored for SBLI flows. It has been validated against experimental data for a range of SBLI configuratins, including high enthalpy ocnditions. The modification to the SU model accounts for capturing the shock-induced unsteadiness in turbulent flows, which lead to improved prediction of turbulence kinetic energy amplification across shocks. A shock unsteadiness parameter and a numerical shock sensor together introduce a shock sensitive correction to the standard $k-\omega$ model.

The governing equations used to solve the flow field incorporate the convective fluxes arising from TCNEQ effects, along with diffusive fluxes, vibrational heat conduction, and source terms for species and vibrational energy. An additional vibrational energy equation is solved to account for the vibrational non-equilibrium, coupled with a five-species chemical non-equilibrium model.

The diffusive flux is modeled using Fick's law, viscosity using Blottner's model and the thermal conductivity by Eucken's relations. Source terms for mass and vibrational energy are expressed using the Arrhenius law and the Landau-Teller model respectively. A detailed description of all the physical models and the SU modified $k-\omega$ model are given in Rathi & Sinha (2024)

These governing equations are solved using the finite volume approach. Inviscid fluxes are calculated via a modified Steger-Warming Flux Splitting technique, while the viscous fluxes are computed using the second-order central difference scheme.

5 RESULTS

5.1 Wall Properties

The wall pressure in Fig.4 is normalized using upstream conditions to enable consistent comparison across different flow cases. The sudden rise in the wall pressure indicates the point of separation. For a fixed wall temperature ratio of 0.3 (H18T30, H24T30, H30T30), increasing stagnation enthalpy from 1.81 MJ/kg to 3.05 MJ/kg delays separation due to higher boundary layer momentum associated with increased freestream velocity and Mach number. The extent of the separation bubble is more clearly captured in the C_f distributions, as shown in Fig.5, where increasing enthalpy results in a reduction of the region of negative C_f Similar trends of decreasing separation extent with increasing enthalpy have been reported by Rathi & Sinha (2024).

The wall temperature also strongly influences separation behavior. A lower wall temperature (H24T15) produces a thinner, denser boundary layer that resists separation, whereas a higher wall temperature (H30T30) leads to a thicker, low-momentum boundary layer that separates faster. This effect is also reflected in the C_f distributions shown in Fig-5, where higher wall temperatures are associated with an extended region of negative C_f, indicating a larger separation bubble. Increasing the wall temperature from 324 K (H24T15) to 648 K (H24T30) and 1296 K (H24T60) leads to a substantial growth of the recirculation region from 13.1 mm to 22.8 mm and 43.7 mm, corresponding to increases of approximately 74% and 91.67%, respectively.

5.2 Interaction Length Scaling

The interaction length scaling used in the present study is based on the formulation proposed by Rathi & Sinha (2024), which builds upon earlier scaling approaches and extends them to high-enthalpy hypersonic turbulent SBLI. The proposed scaling is expressed as

$$L^* = 1.5S_e^4 \quad \text{with} \quad S_e = k\left(\frac{T^*_{ad}}{T^*}\right)^{-0.335}\frac{\Delta p}{q_e} \tag{1}$$

Here L^* is the normalized interaction length calculated as

$$L^* = \frac{L}{\delta^*}\frac{\sin\beta\ \sin\theta}{\sin(\beta-\theta)} \tag{2}$$

T^* is the Eckert's temperature which is a function of wall temperature, recovery temperature and the boundary layer edge temperature upstream of separation. The empirical constant k is equal to 2.5 for all the cases of the current study. Through this formulation, the effects of wall heating and cooling are inherently incorporated into the scaling, enabling more accurate prediction of interaction length in high-enthalpy conditions. L is the interaction length defined as the distance between the foot of separation shock and the flare corner. The displacement thickness δ^* is evaluated from the undisturbed wall-normal velocity profile just upstream of the separation shock. β represents the shock wave angle at the flare corner and θ corresponds to the shock turn angle at the flare corner, obtained using cone shock relations.

The computed values of L^* using Eq.(2) and Se for the present cases are plotted against the scaling relation given in Eq.(1), along with the high and low enthalpy datasets and other datasets from literature in Fig.6. The reference high-enthalpy cases are represented by green and orange squares and diamonds, and present study using pink circles. These cases along with all the other cases mentioned (discussed in Rathi & Sinha (2024)) show a good fit to the scaling law.

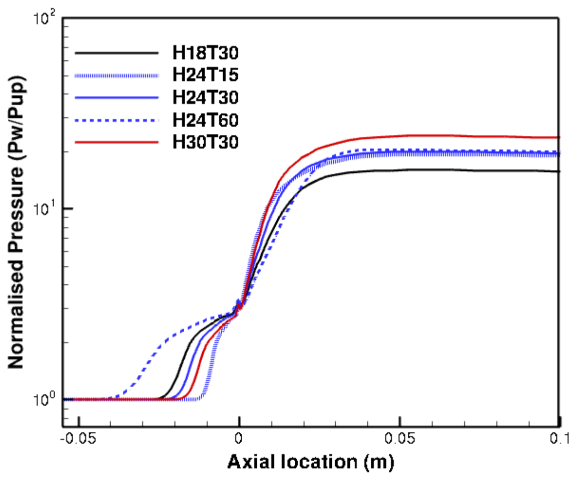

Figure 4. Normalized wall pressure (semilog scale) for cases of the present study listed in Table 1.

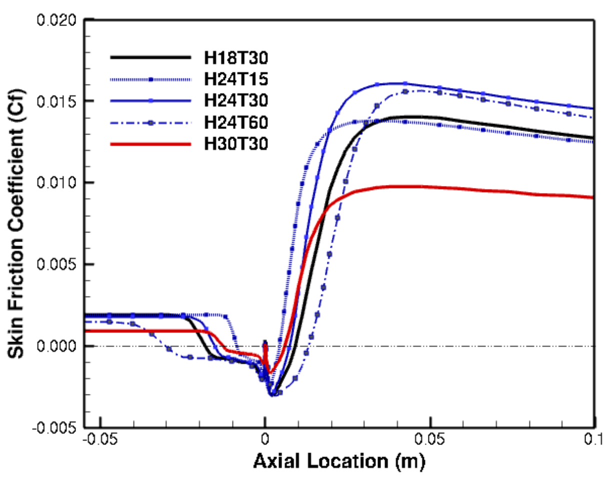

Figure 5. Coefficient of skin friction for the selected cases of the present study listed in Table-1

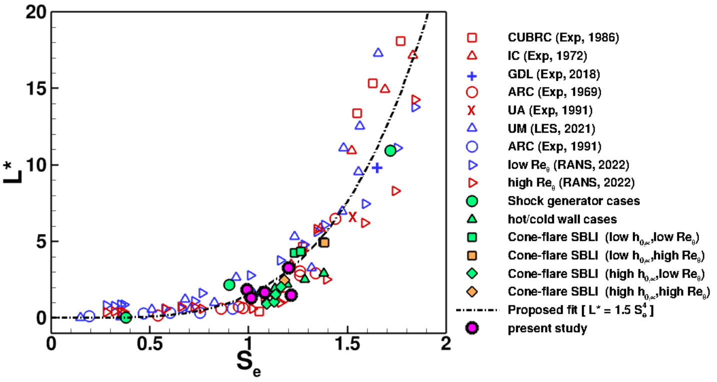

Figure 6. Validation of normalized interaction vs. interaction strength parameter of present study against the proposed scaling (adapted from Rathi & Sinha (2024))

It is observed that the cases H24T15, H24T30 and H24T60, corresponding to increasing wall temperature ratios at constant enthalpy, follow the proposed scaling well. The cases H18T30, H24T30 and H30T30, representing increasing freestream enthalpy at constant wall temperature ratio, show slightly different trend. The low enthalpy case is also close to the scaling curve, while the high enthalpy one shows a larger deviation. Overall, the scaling is found to be adequate in representing the SBLI cases simulated in this work. Larger discrepancies with increasing flow enthalpy may need to be explored further.

5.3 Extension of Scaling Relation

We observe that the case with the highest stagnation enthalpy corresponding to H30T30, shows the largest deviation from the scaling curve. Notably, this case also exhibits the highest gas temperature on the flare, with $T_{\max} \approx 2000$ K. This may serve as a practical upper limit beyond which the scaling relation begins to lose accuracy. This is consistent with the fact that temperatures in the range of 2000-2500 K are typically associated with the onset of chemical non-equilibrium effects (Anderson Jr (1990)). Accordingly, the present study focuses on conditions where T_{max} remains below approximately 2000 K, ensuring that the analysis is primarily within the thermal non-equilibrium but chemical equilibrium regime.

To further investigate this behavior, a simplified method is developed to estimate the maximum temperature in the SBLI using an analytical representation of the incoming turbulent boundary layer. The aim is to obtain a physics-based estimate of T_{max}, which can be compared with CFD results and used to extend the analysis to conditions even ahead of performing the simulations .

In order to accomplish this, the interaction is modeled over the cone–flare configuration by introducing an equivalent oblique shock model with same strength as the cone shock at the flare. Streamlines originating at different y-locations in the undisturbed boundary layer are assumed to pass through the oblique shock generated at the flare corner, as illustrated in Fig. 7,where a simplified configuration without significant flow separation is considered. The boundary layer profiles are estimated analytically for a given shock upstream condition, with the velocity distribution approximated using the classical power-law profile (White (1974)) and the temperature distribution obtained using the Crocco–Busemann relation (Schlichting (2017)), accounting for wall temperature and recovery effects. This provides the wall-normal variation of pre-shock states $\{M_1(y), T_1(y)\}$ within the undisturbed boundary layer. These pre-shock conditions are then used to compute the corresponding post-shock temperature along each streamline using inviscid oblique shock relations, and the maximum temperature within the interaction region is subsequently obtained from the post-shock distribution.

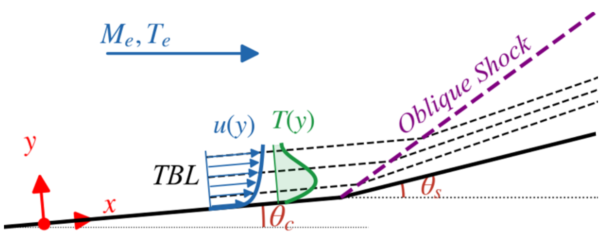

Figure 7. Schematic of cone-flare model used for analytical calculations

It is noted that the boundary layer edge conditions correspond to the post cone shock (shock produced due to 7^0 cone), and therefore the edge Mach number (M_e) and temperature (T_e) differ from the freestream values. A thermally perfect gas formulation with temperature-dependent specific heats is invoked at higher temperatures (Tatum (1996)). Chemical reactions and dissociation effects are neglected. In regions where the local Mach number is insufficient to sustain an attached oblique shock, a detached shock approximation is employed to ensure continuity of the solution.

Fig.8 plots $T_{\max}$ computed using the above procedure for a 33° flare over a range of freestream total enthalpy and wall temperature ratios. As expected, the maximum post-shock temperature increases with both h_0 and T_w/T_r. This trend is attributed to higher upstream boundary layer temperatures associated with increased wall temperature at fixed freestream conditions. It also results from the direct effect of increasing h_0 through higher M_∞, T_∞, or both. The corresponding CFD results for the cases presented in Table-1 are also included, and show excellent agreement with the analytical estimates (error $< 5\%$), thereby validating the proposed procedure.

We next use the limiting value of $T_{\max} = 2000$ K to iden-

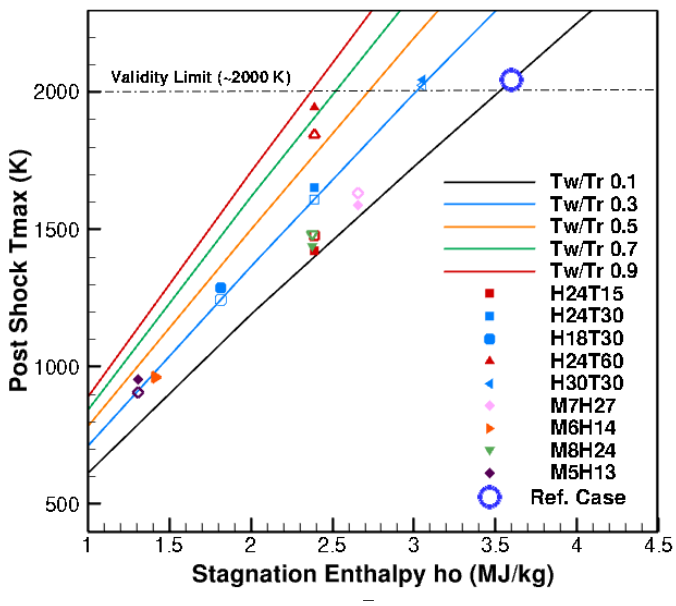

Figure 8. T_{max} vs. h_0 comparison of CFD results (solid- •) and Analytical Model (hollow-○ & ——) for varying T_w/T_r.

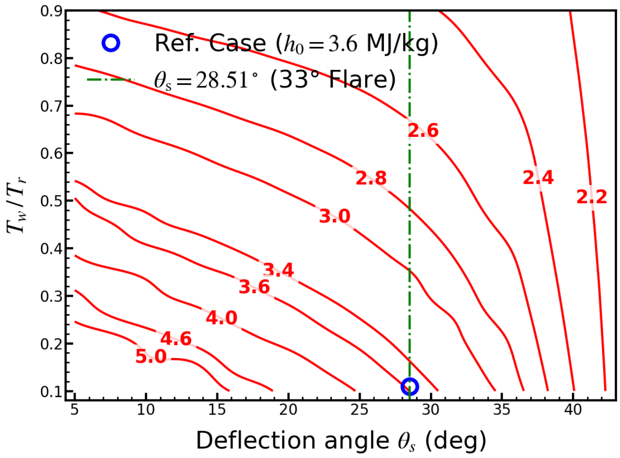

Figure 9. Contour plot showing combinations of θ_s and T_w/T_r for different h_0 corresponding to $T_{\max} \approx 2000$ K.

tify the combinations of h_0 and T_w/T_r that are expected to follow the scaling relation. It is observed that higher enthalpy conditions, such as $h_0 \approx 3.6$MJ/kg, are admissible only under stronger wall cooling corresponding to $T_w/T_r \approx 0.1$ (representing Ref. Case with blue circle in Fig.8 and Fig.9). For higher wall temperature ratios (e.g. $T_w/T_r = 0.7$), the value of h_0 is reduced to 2.5 MJ/kg to follow the scaling law for the cone-flare SBLI.

The analysis is further extended to different flare angles by identifying combinations of T_w/T_r, h_0, and θ_s that yield $T_{\max} \approx 2000$ K as seen in Fig.9. The figure presents iso-$T_{\max}$ contours in the $(\theta_s,\ T_w/T_r)$ plane for different values of h_0. For a specified h_0 and deflection angle θ_s, the corresponding T_w/T_r required to achieve limiting temperature can be directly obtained from these curves. For example, a 33^0 flare angle at $M_\infty = 7$ and $h_0 = 3.6$ MJ/kg, indicates $T_w/T_r \approx 0.1$ on the contour represented by a blue circle (Ref. Case) and is consistent with the corresponding case in Fig.8. It is important to note that θ_s is the shock turn angle calculated using conical shock relations (which is 28.51^0 in this case).

Further, for a fixed h_0, increasing θ_s requires progressively lower T_w/T_r to maintain $T_{\max} \leq 2000$ K and confine to the thermal nonequilibrium regime. If higher values of h_0 are desired at a fixed θ_s, the conditions are limited to lower T_w/T_r in order to remain within the thermal nonequilibrium regime. Therefore, lower flare angles, stronger wall cooling, or both lead to reduced peak temperatures. Conversely, higher enthalpy flows significantly constrain the admissible combinations of θ_s and T_w/T_r, where the scaling relation is expected to remain valid.

Thus each line in Fig.9 (for a given h_0 divides the $\theta_s - T_w/T_r$ plane into two parts. The lower left part (corresponding to smaller deflection and higher wall cooling) has $T_{max} < 2000\ K$. Such cases have thermal nonequilibrium effects, but no chemical reactions and are expected to follow the interaction length scaling given by Eq(1). This suggests that the scaling relation may be extended to significantly higher enthalpy flows than those considered in the present and previous studies. A detailed CFD assessment of these extreme conditions is left for future work.

6 CONCLUSION

In summary, this study presents a systematic investigation of hypersonic turbulent shock–boundary layer interaction (SBLI) with emphasis on the independent variation of freestream total enthalpy and wall temperature ratio. The results show consistent trends in separation behavior, with a reduction in the separation region as enthalpy increases and an increase in separation with higher wall temperature ratios. Interaction length scaling is evaluated under these conditions and is found to capture the overall trends, with increasing deviations observed at higher enthalpy levels.

CFD data for the highest enthalpy test case (H30T30 where $h_0 = 3.05\ MJ/kg$ and $\mathrm{T_w/T_r} = 0.3$) is used to identify a limiting condition where $T_{max} < 2000\ K$ for the maximum temperature in the interaction region. SBLI flows with $T_{max} < 2000\ K$ are expected to have thermal nonequilibrium but no chemical reactions. Such flows are expected to follow the interaction length scaling. A reduced-order model is proposed to predict T_{max}, and it shows a good agreement with CFD data. The model is used to explore the $h_0 - T_W/T_r$ parameter space for cone-flare flows to identify the flare angles which are amenable to the interaction length scaling available in literature.

Overall, the proposed framework provides a structured approach to assess SBLI behavior and extend scaling relations across a wider range of high-enthalpy conditions, indicating the need of further exploration at higher enthalpies.

REFERENCES

Anderson Jr, John D 1990 Non-equilibrium chemistry effects on hypersonic separated flows–shock-wave/boundary-layer interaction. *Tech. Rep.*.

Boyce, Russell, Gerard, Sullivan & Paull, Allan 2003 The hyshot scramjet flight experiment-flight data and cfd calculations compared. In *12th AIAA international space planes and hypersonic systems and technologies*, p. 7029.

Duan, Lian & Martin, MP 2011 Direct numerical simulation of hypersonic turbulent boundary layers. part 4. effect of high enthalpy. *Journal of Fluid Mechanics* **684**, 25–59.

Jiang, Hao, Liu, Jun, Luo, Shichao, Huang, Wei, Wang, Junyuan & Liu, Meikuan 2022 Thermochemical non-equilibrium effects on hypersonic shock wave/turbulent boundary-layer interaction. *Acta Astronautica* **192**, 1–14.

Kimmel, Roger, Adamczak, David, Berger, Karen & Choudhari, Meelan 2010 Hifire-5 flight vehicle design. In *40th Fluid Dynamics Conference and Exhibit*, p. 4985.

Passiatore, Donatella, Sciacovelli, Luca, Cinnella, Paola & Pascazio, G 2022 Thermochemical non-equilibrium effects in turbulent hypersonic boundary layers. *Journal of Fluid Mechanics* **941**, A21.

Rathi, Harsha & Sinha, Krishnendu 2024 Interaction length analysis of hypersonic shock–boundary-layer interaction including high-enthalpy effects. *AIAA Journal* pp. 1–18.

Schlichting, Kluas Gersten 2017 *Boundary-Layer Theory*. Springer.

Tatum, Kenneth E 1996 Computation of thermally perfect properties of oblique shock waves. *Tech. Rep.*.

Volpiani, Pedro Stefanin 2021 Numerical strategy to perform direct numerical simulations of hypersonic shock/boundary-layer interaction in chemical nonequilibrium. *Shock Waves* **31** (4), 361–378.

White, Frank M. 1974 *Viscous FLuid Flow*. McGraw Hill.